Free vibrations of a spherical drop constrained at an azimuth

Cite as: Phys. Fluids **24**, 082102 (2012); https://doi.org/10.1063/1.4742339
Submitted: 26 July 2011 . Accepted: 09 July 2012 . Published Online: 10 August 2012

Santhosh Ramalingam, Doraiswami Ramkrishna, and Osman A. Basaran

Free vibrations of a spherical drop constrained at an azimuth

Santhosh Ramalingam,[a] Doraiswami Ramkrishna, and Osman A. Basaran[b]
School of Chemical Engineering, Purdue University, West Lafayette, Indiana 47907, USA

(Received 26 July 2011; accepted 9 July 2012; published online 10 August 2012)

Two droplets coupled through a liquid filled (a) hole in a plate or (b) tube is referred to as a double droplet system (DDS) or a capillary switch. Such capillary systems are gaining increasing attention due to their utility in applications. A particularly exciting application is one where a DDS is employed as a liquid lens, one flavor of which entails using a DDS as a variable focus lens by keeping it under sustained oscillations at its natural frequencies. The natural modes of oscillation of a DDS are determined analytically here in the limit in which the plate thickness (or tube length) is vanishingly small and when the effect of gravity is negligible compared to that of surface tension. In this limit, a DDS at rest reduces to two spherical caps that are pinned to and coupled along a common circular ring of contact of negligible thickness. Here, the caps are taken to be complementary pieces of a sphere so that the equilibrium state of the system is a sphere that is constrained by a ring of negligible thickness at an azimuthal angle with respect to the center of the sphere. Both the constrained drop and the fluid exterior to it are taken to be inviscid fluids undergoing irrotational flow. Similar to the linear oscillations of a free drop first studied by Rayleigh, the analytical formulation of the linear oscillations of the constrained drop results in a linear operator eigenvalue problem but with one additional boundary condition, i.e., that which accounts for zero shape perturbation along the circle of contact. Exploiting properties of linear operators, an implicit expression is obtained for the frequency of each mode of oscillation, a feat that appears not to have been accomplished to date in any problem involving oscillations of constrained drops. An extension of a method based on Green's functions that was developed to analyze the linear oscillations of a drop in contact with a spherical bowl [M. Strani and F. Sabetta, "Free-vibrations of a drop in partial contact with a solid support," J. Fluid Mech. **141**, 233–247 (1984)] is also employed to verify the aforementioned results. Results obtained from these two approaches are then compared to those reported by Bostwick and Steen ["Capillary oscillations of a constrained liquid drop," Phys. Fluids **21**, 032108 (2009)]. Careful examination of flow fields within drops reveals that by pinning a drop, it should be possible to selectively excite just a portion of a drop's surface. © *2012 American Institute of Physics*. [http://dx.doi.org/10.1063/1.4742339]

I. INTRODUCTION

Interest in the oscillations of drops can be traced to the works of some of the 19th century giants of physical science (see the review provided by Scriven[1]), the most well known of these being the paper by Lord Rayleigh[2] in which he theoretically determined the frequencies of infinitesimal-amplitude oscillations of a free drop of an inviscid fluid that is surrounded by a dynamically passive gas. Over the years, researchers have built on the pioneering work of Rayleigh by considering the effects of small

[a]Present address: The Dow Chemical Company, Freeport, Texas 77566, USA.
[b]obasaran@purdue.edu.

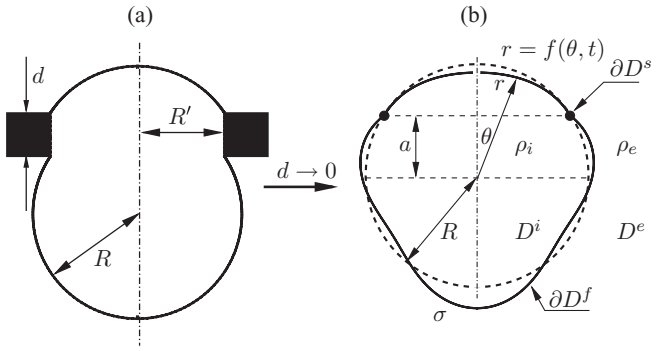

FIG. 1. (a) A capillary switch (CS) or a double droplet system (DDS) is a coupled interface system wherein a sessile drop and a pendant drop are coupled through a fluid filled hole in a plate or a tube. Here, R' is the hole or tube radius, d is the plate thickness or tube length, and R is the radius of curvature of the spherical caps. (b) When $d \to 0$, a CS or a DDS reduces to a drop that is pinned at an azimuth by a circular ring of vanishingly small thickness.

viscosity,[3] finite viscosity,[4] drop rotation,[5,6] a dynamically active ambient fluid,[7–9] finite-amplitude oscillations,[10–13] and surface-active species at the drop-ambient fluid interface.[14] In the last few decades of the 20th century, researchers have also started to consider situations in which an oscillating drop is attached to a tube or a solid surface. These oscillating pendant and sessile drop problems were motivated by practical applications in fields as diverse as surface tension measurement,[15] separations,[16] printing,[17] and mixing, heat transfer, and mass transfer enhancement.[18,19]

Motivated by applications in microfluidics, biology, and optics, more recently attention has shifted from these earlier studies of single drop systems consisting of either simple free drops or supported drops to ones involving coupled drops.[20] A distinguished example of a system involving coupled drops is a capillary switch (CS), wherein a sessile drop and a pendant drop are simply coupled through a fluid filled hole in a plate or a tube,[21] as shown in Fig. 1(a). The sessile and the pendant drops are pinned to the two ends of the hole or the tube and surrounded by a dynamically passive gas that exerts a spatially uniform pressure p_s and p_p on the two drops. When the Bond number $G \equiv \rho g R'^2/\sigma \ll 1$, where ρ, g, R', and σ stand for the density of the liquid, the acceleration due to gravity, the hole or tube radius, and the surface tension of the liquid-gas interface, the equilibrium shapes of both drops are sections of spheres or spherical caps. If $p_s = p_p$, the double droplet system (DDS) is known to have one or three equilibrium shapes depending on whether the combined volume of the sessile and the pendant drops, V_s and V_p, is smaller or larger than a critical volume $(4/3)\pi R'^3$ equal to that of a sphere having the same radius as the hole or the tube.[21] Below this critical volume, the system has a single equilibrium state such that both drops have identical subhemispherical shapes and the equilibrium state is stable. Above this critical volume, the system has two stable equilibrium shapes and one unstable shape, and therefore exhibits bistable behavior. The unstable equilibrium state is such that both drops have identical superhemispherical shapes. The two stable equilibrium states are such that the two unequal spherical caps are complementary pieces of a sphere. In the limit of vanishingly small plate thickness or tube length d, the DDS (or CS) reduces to two spherical caps that are pinned to and coupled along a common circular ring of contact of negligible thickness. In this paper, the caps are taken to be complementary pieces of a sphere so that the equilibrium state of the system is a sphere that is constrained by a ring of negligible thickness at an azimuthal angle with respect to the center of the sphere, as shown in Fig. 1(b). A major goal of this paper is to advance the understanding of the natural modes of oscillations of such constrained spherical drops.

In the absence of a ring, if a free or isolated spherical drop of an incompressible inviscid fluid that is immersed in another incompressible inviscid fluid is subjected to infinitesimal-amplitude perturbations, it will undergo linear oscillations. For axisymmetric motions, the drop's response can be characterized by a countably infinite number of modes (eigenmodes), $n = 2, 3, 4, \ldots$, such that the shape of each mode is proportional to the Legendre polynomial P_n of order n. For each mode, often referred to as a Rayleigh mode, the drop oscillates or undergoes Rayleigh oscillations with a

frequency (eigenfrequency), often referred to as a Rayleigh frequency, given by

$$\omega_n^2 = \frac{n(n-1)(n+1)(n+2)}{(n+1)\rho_i + n\rho_e}\frac{\sigma}{R^3}, \tag{1}$$

where σ, ρ_i, ρ_e, and R denote the surface tension, the density of the drop or interior fluid, the density of the ambient or exterior fluid, and the radius of the undeformed drop, respectively. For oscillations of free drops, the lowest realizable mode corresponds to $n = 2$ because the modes corresponding to $n = 0$ and $n = 1$ do not arise as they represent disallowed motions that would violate the condition of volume conservation and cause the drop's center-of-mass to move, respectively. It is noteworthy that the equations governing these linearized oscillations reduce to a linear operator eigenvalue problem subject to a volume constraint and boundedness of the perturbations at the two poles.

When the spherical drop of the previous paragraph is constrained by either a spherical bowl of equal radius to the drop (Strani and Sabetta, 1984),[22] or by a ring of vanishingly small thickness (Bostwick and Steen, 2009[23]) the linear modes of oscillation and their frequencies are governed by the same linear operator problem that governs the Rayleigh modes and their frequencies. However, in addition to the volume constraint and the boundedness conditions, the linear operator in this case is also constrained by the vanishing of perturbations along the solid contact. Strani and Sabetta developed the appropriate Green's functions of the linear operator and expressed the mode shapes in Legendre polynomial series, which allowed them to reduce the governing equation to a matrix eigenvalue problem. The resulting eigenvalues and eigenvectors correspond to the frequencies and shapes of the various modes of oscillation. Bostwick and Steen[23] showed that the ring constraint, when projected onto a meridional plane, reduces to a point contact and hence judiciously picked a set of basis functions, h_n, as linear combinations of P_n and P_1, $n \geq 2$, viz., $h_n = \alpha_n P_n + \beta_n P_1$ (where α_n and β_n are unknown coefficients), such that these new basis functions satisfied the boundary condition at the ring. An orthonormal basis function set was then created using the Gram-Schmidt method. By expressing the shape perturbation as a linear combination of these orthonormal basis functions, they were able to reduce the linear operator problem to a matrix equation which was eventually solved to obtain the eigenvalues. Among other things, Bostwick and Steen's work helped clarify the physics of center-of-mass motion in problems involving constrained drops. Since the motion of the center-of-mass is completely determined by the disallowed $n = 1$ mode for free drops, it had heretofore been believed incorrectly that this was also the case for constrained drops. Bostwick and Steen[23] clearly showed that while the $n = 1$ mode carries the majority of the center-of-mass motion, the higher mode shapes are also accompanied by an associated motion of the drop's center-of-mass.

By contrast to the aforementioned studies of oscillations of constrained drops, numerical methods have been the tools of choice in almost all previous studies of oscillations of constrained drops such as pendant and sessile drops that are suspended from tubes or supported by solid substrates. The use of numerical methods in such studies has often been necessitated because of the lack of spherical symmetry in these problems. In a series of papers, Basaran and co-workers have used finite element based approaches to study the free and forced oscillations of viscous pendant and sessile drops undergoing linear as well as highly nonlinear motions.[16,17,24,25] An exception to such numerical approaches is the work of Lyubimov *et al.*[26] who have theoretically studied the linearized oscillations of a hemispherical pendant drop of an inviscid fluid that makes a fixed contact angle with the supporting plate. Recently, Theisen *et al.*[27] have modeled the small-amplitude oscillations of capillary switches by *a priori* restricting the transient drop shapes to be sections of spheres. While their experiments have shown that the model's predictions are quite accurate at small amplitudes, these authors have also shown that non-spherical shapes are observed during large-amplitude oscillations. This model has also been extended by Slater *et al.*[28] to study large-amplitude oscillations. More recently, Ramalingam and Basaran[29] have used a finite element based approach to determine the modal shapes and modal frequencies of capillary switches of volumes less than the critical value of $(4/3)\pi R'^3$ that are undergoing linear oscillations without invoking the spherical cap approximation.

The subject of this paper is the infinitesimal-amplitude, axisymmetric oscillations of a drop of an inviscid fluid that is constrained by a ring of infinitesimal thickness at a latitude and surrounded by another inviscid fluid. The system under consideration is identical to that considered by Bostwick

and Steen.[23] While the system and, therefore, the mathematical statement of the problem is the same as theirs, the emphasis of this paper is to present two other solution techniques to solve the resulting constrained eigenvalue problem. The first technique recasts the eigenvalue problem into a Rayleigh-Ritz type minimization problem and seamlessly incorporates the fixed point constraint by means of a Lagrange multiplier. The mode shapes given by the functions that minimize the objective function and satisfy the necessary constraints are obtained as a series expansion of Legendre polynomials. After a few simple algebraic manipulations, an implicit expression is derived for the frequency of each mode of oscillation which, to our knowledge, has heretofore not been reported in any theoretical study involving the oscillations of a constrained drop. The second technique is a direct extension of Strani and Sabetta's method but is differentiated from their approach in that Green's functions in the present paper are modified to satisfy the fixed point constraint. These two approaches are described in detail in subsequent sections of the paper.

The paper is then organized as follows. In Sec. II, the derivation of the linear operator eigenvalue problem is provided. Although some of this material can be found in both the papers by Strani and Sabetta[22] and Bostwick and Steen,[23] it is included here for completeness and also because it is necessary to enable the reader to follow the analyses in subsequent sections. Sections III and IV describe the minimization and Green's function methodologies in detail. In Sec. V, the correctness of the two new approaches is verified by comparing the frequencies and mode shapes predicted by one method against predictions made by the other and also by Bostwick and Steen.[23] Certain salient points of the work and its implications are then summarized in Sec. VI.

II. MATHEMATICAL FORMULATION

The system is isothermal and consists of a drop of an inviscid fluid that is constrained by a ring of negligible thickness and is surrounded by another immiscible inviscid fluid. The effect of gravity is neglected so that the equilibrium shape of the drop is a sphere of radius R. The goal is to analyze the axisymmetric oscillations of infinitesimal-amplitude of the drop such that the flow is incompressible and irrotational both inside and outside the drop. Thus, the drop and exterior fluid densities are both constants and denoted by ρ_i and ρ_e, and the interfacial tension of the interface separating the two phases is also constant and denoted by σ. In what follows, i and e as subscripts (superscripts) are used to differentiate the material (field) properties of the drop and surrounding fluids. Due to the axial symmetry of the dynamics and the spherical symmetry of the base state, it proves convenient to use a spherical polar coordinate system (r, θ, ψ), where r, θ, andψ stand for the radial coordinate, the cone angle, and the polar angle, with its origin at the center of the unperturbed drop. The system is projected onto a meridional plane (r-θ plane) as shown in Figure 1 in which the solid contact is reduced to a point contact at a certain azimuthal angle α or, equivalently, at an axial distance a from the center of the drop, on the free surface.

In the absence of any perturbations, both fluids are quiescent, the drop shape is spherical, and the pressure in both fluids are spatially invariant with the drop pressure exceeding the external pressure by $2\sigma/R$. The equations and boundary conditions governing the dynamics are derived by first expressing the velocity $\mathbf{V}(r, \theta, t)$, pressure $P(r, \theta, t)$, and the drop shape $r = f(\theta, t)$, where t is time, as the undisturbed or base state value, viz., $\mathbf{v}_0$, p_0, and R, plus a perturbation

$$\mathbf{V} = \mathbf{v}_0 + \mathbf{v} = \mathbf{0} + \mathbf{v}, \tag{2}$$

$$P = p_0 + p, \tag{3}$$

$$f = R + \eta, \tag{4}$$

where $\mathbf{v}$, p, and η stand for small perturbations.

Since the velocity field is irrotational, the perturbation velocity is given by the negative of the gradient of a scalar velocity potential, viz., $\mathbf{v} = -\nabla\Phi$. It then follows from the continuity equation for incompressible flow that the velocity potential is governed by Laplace's equation

$$\nabla^2\Phi = \sin\theta(r^2\Phi_r)_r + (\sin\theta\,\Phi_\theta)_\theta = 0 \tag{5}$$

in

$$D^i \equiv \{(r,\theta)|0 \le r \le f, 0 \le \theta \le \pi\},$$
$$\text{and } D^e \equiv \{(r,\theta)|f \le r \le \infty, 0 \le \theta \le \pi\}, \tag{6}$$

where D^i and D^e stand for the regions interior and exterior to the drop. Here and throughout the remainder of the paper, subscripts r, θ, t denote partial differentiation with respect to those variables.

From Euler's equations of motion, it is readily shown that the disturbance pressure in each phase is governed by a linearized Bernoulli equation

$$p = \rho\Phi_t \text{ in } D^i \text{ and } D^e. \tag{7}$$

Whereas Eqs. (5) and (7) ensure mass and momentum conservation within the bulk fluids, their counterparts along the drop surface are of course the linearized traction and kinematic boundary conditions

$$p^i - p^e = -\sigma\frac{1}{R^2}\left(\frac{(\sin\theta\eta_\theta)_\theta}{\sin\theta} + 2\eta\right) \quad \text{on } \partial D^f, \tag{8a}$$

$$\Phi_r = -\eta_t \quad \text{on } \partial D^f, \tag{8b}$$

where

$$\partial D^f \equiv \{(r,\theta)|r = f, 0 \le \theta \le \pi, \theta \ne \alpha\}. \tag{9}$$

The pressures appearing above are eliminated below in favor of the velocity potentials by means of Bernoulli's equation.

Along the solid circle of contact, the no penetration condition requires that

$$\Phi_r = -\eta_t = 0 \text{ on } \partial D^s, \tag{10}$$

where

$$\partial D^s \equiv \{(r,\theta)|r = f, \theta = \alpha\}. \tag{11}$$

Finally, the surface perturbation must leave the drop volume unchanged, viz.,

$$\int_0^\pi \eta \sin\theta d\theta = 0. \tag{12}$$

Using normal mode analysis, the velocity potential and the perturbation to the drop shape are written as

$$\Phi = \phi(r,\theta)e^{i\omega t}, \tag{13}$$

$$\eta = z(\theta)e^{i(\omega t+\pi/2)}, \tag{14}$$

where ω is the frequency and the phase difference $\pi/2$ ensures that the traction and kinematic boundary conditions are satisfied. The system of Eqs. (5), (8a), (8b), and (10) is then written in terms of amplitude or the reduced functions ϕ and z using Eqs. (13) and (14) resulting in

$$\nabla^2\phi = 0 \quad \text{in } D, \tag{15a}$$

$$\phi_r = \omega z \quad \text{on } \partial D^f, \tag{15b}$$

$$\omega(\rho_i\phi^i - \rho_e\phi^e) = -\frac{\sigma}{R^2}\left(\frac{(\sin\theta z_\theta)_\theta}{\sin\theta} + 2z\right) \quad \text{on } \partial D^f, \tag{15c}$$

$$\phi_r = 0 \quad \text{on } \partial D^s. \tag{15d}$$

The above set of equations can be recognized to be equivalent to the standard Neumann problem. Making the change of variable $x = \cos\theta$, and imposing the kinematic boundary condition

(15b) and boundedness conditions at the poles, the time independent velocity potentials ϕ can be written as

$$\phi^i = \omega R \left(\phi_0 + \sum_{k=1}^{\infty} \frac{\phi_k}{k} \frac{r^k}{R^k} p_k(x) \right), \tag{16}$$

$$\phi^e = -\omega R \sum_{k=1}^{\infty} \frac{\phi_k}{k+1} \frac{R^{k+1}}{r^{k+1}} p_k(x), \tag{17}$$

where $p_k(x)$ is the normalized kth Legendre polynomial, and the coefficients ϕ_k are given by

$$\phi_k = < z, p_k > \tag{18}$$

with the inner product defined as

$$< f, g > = \int_{-1}^{1} fg \, dx. \tag{19}$$

Substituting Eqs. (16) and (17) in the traction boundary condition (15c), the surface perturbation equation can be shown to satisfy a second order integro-differential equation given by

$$[(1-x^2)z_x]_x + 2z = -\frac{\rho^i \omega R^2}{\sigma} \left[\phi_0 + \sum_{k=1}^{\infty} \beta_k \phi_k p_k \right], \tag{20}$$

where

$$\beta_k = \frac{1}{k} + \frac{\rho_e}{\rho_i} \frac{1}{k+1}. \tag{21}$$

Solutions to Eq. (20) need to be calculated subject to the volume constraint, boundedness conditions at the poles and vanishing of the perturbation at the solid contact

$$\int_{-1}^{1} z(x) dx = 0, \tag{22a}$$

$$z(a) = 0; \qquad a = \cos\alpha, \tag{22b}$$

$$z(\pm 1) \quad \text{is finite.} \tag{22c}$$

Equation (20) is conveniently written as a linear operator eigenvalue problem

$$\mathbf{L}z = \lambda \mathbf{M} z, \tag{23}$$

where

$$\mathbf{L}\bullet = -\frac{d}{dx}\left[(1-x^2) \frac{d\bullet}{dx} \right] - 2(\bullet), \tag{24a}$$

$$\mathbf{M}\bullet = < \bullet, p_0 > + \sum_{k=1}^{\infty} \beta_k < \bullet, p_k > p_k, \tag{24b}$$

$$\lambda = \frac{\rho_i \omega^2 R^3}{\sigma}. \tag{24c}$$

The second order linear differential operator $\mathbf{L}$ can readily be identified as the Legendre differential operator, which along with boundary conditions (22b) and (22c) is a self-adjoint operator for differentiable functions in $[-1, 1]$ under the inner product defined by Eq. (19). $\mathbf{M}$ is a self-adjoint

positive definite operator in the same domain. Solutions to Eq. (23) that satisfy constraints (22) are the eigenfunctions describing the shapes of unique modes of oscillations that undergo periodic motion with a non-dimensional frequency $\sqrt{\lambda}$. In (24c) and elsewhere in the paper, dimensionless frequencies are measured in units of $\sqrt{\sigma/\rho_i R^3}$.

As mentioned earlier, all three drop oscillation problems (Rayleigh,[2] Strani and Sabetta,[22] and Bostwick and Steen[23]) aim to find the eigenvalues and eigenfunctions of Eq. (23) subject to a volume constraint and other problem specific constraints.

III. MINIMIZATION METHOD

Consider the linear differential operator $\mathbf{L}$ and the operator $\mathbf{M}$ from Eq. (24) with dense linear domains given by differentiable functions $z(x)\,\forall\, x \in [-1, 1]$ such that

$$\int_{-1}^{1} z(x)dx = 0; \qquad z(a) = 0. \tag{25}$$

A major goal of this section is to find the eigenvalues of the operator $\mathbf{T} = \mathbf{M}^{-1}\mathbf{L}$. It can be easily shown that the operator $\mathbf{T}$ is self-adjoint[30] with respect to the inner product defined in $\mathcal{L}^2[-1, 1]$ by

$$\langle u, v\rangle_M = \langle \mathbf{M}u, v\rangle,$$

where $\langle\ ,\ \rangle$ is the inner product as per Eq. (19). It is worth noting that the linear self-adjoint operators $\mathbf{L}$ and $\mathbf{M}$ (under normal inner product) have eigenvalues $\gamma_j = (j-1)(j+2)$ and β_j (21), respectively, with the normalized Legendre polynomial p_j as the corresponding eigenfunction. Therefore, the linear operator $\mathbf{T}$ has eigenvalues γ_j/β_j with p_j as the corresponding eigenfunctions. Equation (23) can be equivalently written in Rayleigh-Ritz form as

$$\mathbf{L}z = \lambda\mathbf{M}z \;\equiv Min\left[\langle \mathbf{T}z, z\rangle_M - \lambda(\langle z, z\rangle_M - 1)\right]. \tag{26}$$

In the presence of a solid contact, as in this problem, the constraint is included in the formulation by introducing an additional Lagrange multiplier ν. The eigenvalue λ may then be determined by minimization of the objective function as

$$Min\left[\langle \mathbf{T}z, z\rangle_M - \lambda(\langle z, z\rangle_M - 1) - \nu z(a)\right].$$

The objective function is simplified by expanding $z(x)$ in terms of normalized Legendre polynomials

$$z(x) = \sum_{j=1}^{N} c_j p_j(x). \tag{27}$$

The number of polynomials in the expansion, N, is determined by increasing its value until further increases in N result in negligible changes in the eigenvalues and eigenfunctions. Exclusion of the p_0 term automatically ensures that the volume constraint is satisfied. Each term in the objective

function is calculated as

$$\begin{aligned}
\langle \mathbf{T}z, z\rangle_M &= \langle \mathbf{MT}z, z\rangle \\
&= \langle \mathbf{L}z, z\rangle \\
&= \int_{-1}^{1} \sum_{j=1}^{N} c_j \gamma_j p_j(x) \sum_{k=1}^{N} c_k p_k(x) dx \\
&= \sum_{j=1}^{N} c_j^2 \gamma_j, \\
\langle z, z\rangle_M &= \sum_{j=1}^{N} c_j^2 \beta_j, \\
z(a) &= \sum_{j=1}^{N} c_j p_j(a).
\end{aligned}$$

The reduced minimization problem is then rewritten as

$$Min \left\{ \sum_{j=1}^{N} c_j^2 \gamma_j - \nu \sum_{j=1}^{N} c_j p_j(a) - \lambda \left(\sum_{j=1}^{N} c_j^2 \beta_j - 1 \right) \right\}. \tag{28}$$

Differentiating with respect to c_k and setting the result equal to zero gives

$$2\gamma_k c_k - \nu p_k(a) - 2\lambda \beta_k c_k = 0$$

$$\Rightarrow c_k = \frac{\nu p_k(a)}{2(\gamma_k - \lambda \beta_k)}. \tag{29}$$

The normalization condition $\langle z, z\rangle_M = 1$ yields

$$\sum_{k=1}^{N} \frac{\nu^2 \beta_k p_k^2(a)}{4(\gamma_k - \lambda \beta_k)^2} = 1$$

$$\Rightarrow \nu = \frac{2}{\sqrt{\sum_{k=1}^{N} \frac{\beta_k p_k^2(a)}{(\gamma_k - \lambda \beta_k)^2}}}. \tag{30}$$

Substitution of Eqs. (29) and (30) in the fixed contact constraint $z(a) = 0$ leads to an implicit expression for the eigenvalues

$$f(\lambda) \equiv \sum_{k=1}^{N} \frac{p_k^2(a)}{(\gamma_k - \lambda \beta_k)} = 0, \tag{31}$$

which, however, must be solved numerically for the eigenvalues.

Figure 2 shows the variation of $f(\lambda)$ with λ for a given value of the location of the ring constraint, $a = 0.5$, and a fixed value of the number of polynomials used in (27), $N = 100$. First, as can be readily seen from (31), $f(\lambda)$ has a pole at $\lambda = \gamma_k/\beta_k$ for each $k \geq 0$. Second, $f(\lambda)$ is a monotonically increasing function of λ and varies from $-\infty$ to $+\infty$ between two successive poles. Therefore, there exists one and only one zero of $f(\lambda)$ between two consecutive poles, whose location corresponds to an eigenvalue, λ. It should also be noted that γ_k/β_k is the square of the dimensionless frequency of the kth mode of oscillation of a free drop (Rayleigh oscillation), and hence the frequency of the kth mode for the ring constrained drop, $\sqrt{\lambda_k}$, lies between the kth and $(k+1)$th Rayleigh frequencies. While Strani and Sabetta showed that the frequency of oscillation of a particular mode of a constrained drop is bounded below by the same mode frequency of a free drop, Bostwick and Steen[23] showed

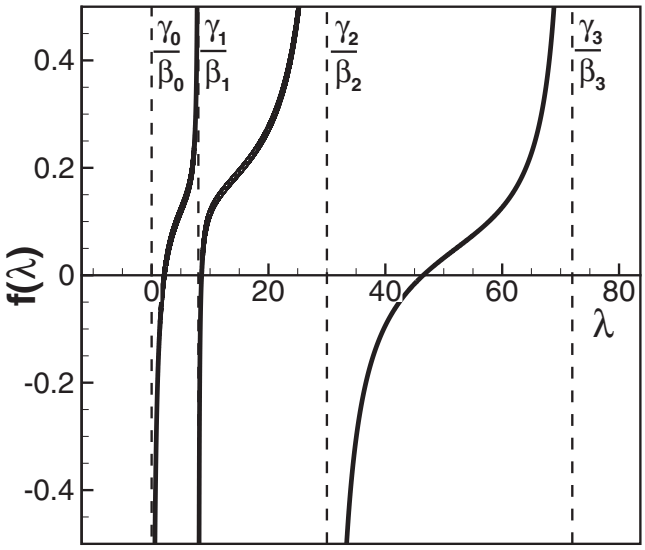

FIG. 2. Figure for illustrating the properties of the function $f(\lambda)$ used in Eq. (31). In this figure, $\rho_e \ll \rho_i \equiv \rho$. Here, results are shown for the situation in which $a = 0.5$ and $N = 100$. The vertical dotted lines $- - -$ represent the poles of $f(\lambda)$ which also correspond to the eigenvalues of the Rayleigh modes.

that it is bounded above by the frequency of the next higher mode of a free drop. Hence, Eq. (31) theoretically proves these bounds. For each mode of oscillation, the modal shape, $z_k(x)$, can be obtained by substituting the value λ_k in Eqs. (29) and (30).

IV. GREEN'S FUNCTION METHOD

Since the operator $\mathbf{L}$ is linear and self-adjoint under the inner product defined in Eq. (19), the solution to Eq. (23) can also be found by Green's function method. The methodology adopted in this paper and that is described in this section is a direct extension of the approach used by Strani and Sabetta[22] in their study of the inviscid oscillations of a spherical drop in partial contact with a spherical bowl having the same radius as the drop. While Strani and Sabetta used a single Green's function such that this function equaled zero over the portion of the drop in contact with the bowl and was non-zero over free surface of the drop, here a composite Green's function is used in the analysis. The composite function consists of two non-zero Green's functions, one for each free surface, i.e., the free surface above and the free surface below the contact point. If $G(x, y)$ is Green's function for the operator $\mathbf{L}$ in $[-1, 1]$, then the solution to Eq. (23) is given by

$$z(x) = \lambda \int_{-1}^{1} G(x, y)\mathbf{M}z(y)dy. \tag{32}$$

A. Construction of Green's function

For a linear self-adjoint operator with unmixed boundary conditions, Green's function is easily constructed from the homogeneous solutions of the governing differential equation.[30] Green's function for the operator $\mathbf{L}$ is constructed from the solutions to the homogeneous differential equation $\mathbf{L}z = 0$, which is readily recognized as the Legendre differential equation of order one. Hence, the homogeneous solutions are given by

$$\begin{aligned} P_1(x) &= x, \\ Q_1(x) &= \frac{x}{2}\log\left(\frac{1+x}{1-x}\right) - 1, \end{aligned} \tag{33}$$

where $P_1(x)$ and $Q_1(x)$ are the order one Legendre functions of the first and second kinds, respectively.

In the present problem, the governing differential equation is to be solved subject to not only the regular boundedness conditions at $x = \pm 1$ but also to the pinning condition due to the presence of the ring constraint

$$z(-1) \quad \text{is bounded,} \tag{34a}$$

$$z(a) = 0, \tag{34b}$$

$$z(1) \quad \text{is bounded.} \tag{34c}$$

The additional constraint at the contact point is incorporated into the formulation by dividing the domain into two sub-domains, $[-1, a] \cup [a, 1]$, and constructing a composite Green's function as

$$G(x, y) = \begin{cases} G_1(x, y) & \text{for x,y} \in [-1, a] \times [-1, a] \\ G_2(x, y) & \text{for x,y} \in [a, 1] \times [a, 1]. \end{cases} \tag{35}$$

Thus, G_1 is constructed with boundary conditions (34a) and (34b), whereas G_2 is constructed with (34b) and (34c). The derivation of the appropriate Green's functions with the above unmixed boundary conditions is straightforward and yields

$$G_1(x, y) = \begin{cases} -P_1(y)\left(Q_1(x) - \frac{P_1(x)Q_1(a)}{a}\right) & \text{for } -1 \le y \le x \le a \\ -P_1(x)\left(Q_1(y) - \frac{P_1(y)Q_1(a)}{a}\right) & \text{for } -1 \le x \le y \le a, \end{cases} \tag{36a}$$

$$G_2(x, y) = \begin{cases} P_1(x)\left(Q_1(y) - \frac{P_1(y)Q_1(a)}{a}\right) & \text{for } a \le y \le x \le 1 \\ P_1(y)\left(Q_1(x) - \frac{P_1(x)Q_1(a)}{a}\right) & \text{for } a \le x \le y \le 1. \end{cases} \tag{36b}$$

It can be readily seen that the pinned contact boundary condition is satisfied when the above Green's function is substituted into Eq. (32).

B. Solution procedure

Expressing the surface perturbation $z(x)$ and Green's function $G(x, y)$ in Legendre polynomial series, Eq. (32) can be reduced into matrix form as

$$z_h = \lambda \sum_{l=1}^{\infty} \beta_l \left(\mathbf{G}_{hl} - \frac{\mathbf{G}_{0l}\mathbf{G}_{h0}}{\mathbf{G}_{00}}\right) z_l, \tag{37}$$

where

$$z_h = < z, p_h >,$$
$$G_{hl} = \langle \langle G, p_h \rangle, p_l \rangle.$$

For computational reasons, the order of the polynomial approximation is restricted to a finite integer N whose value is then determined by the same criterion as that already discussed in Sec. III on the minimization method. Equation (37) can be written as a standard matrix eigenvalue problem

$$\mathbf{A}\zeta = \alpha\zeta \tag{38}$$

using the change of variables $\zeta_k = \sqrt{\beta_k} z_k$ and $\alpha = 1/\lambda$. The methodology of converting the linear operator problem (23) into a matrix eigenvalue problem involving the Green's function has been described in detail by Strani and Sabetta. Therefore, a condensed version of this analysis appropriate to the present problem is reported in the Appendix.

The coefficients $\mathbf{G}_{hl}$ can be calculated from well-known properties of Legendre polynomials. When $l \neq 1$, the following identities[31] can be used to simplify the coefficients G_{hl},

$$\int_x^1 P_h(y)P_l(y)dy = \frac{h\,P_l(x)P_{h-1}(x) - l\,P_h(x)P_{l-1}(x) - (h-l)x\,P_h(x)P_l(x)}{(h-l)(h+l+1)},$$

$$\int_x^1 Q_h(y)P_l(y)dy = \frac{h\,P_l(x)Q_{h-1}(x) - l\,Q_h(x)P_{l-1}(x) - (h-l)x\,Q_h(x)P_l(x)}{(h-l)(h+l+1)}.$$

After some straightforward algebra, it can be shown that

$$\mathbf{G}_{hl} = \mathbf{G}_{lh} = \frac{1}{a(l-1)(l+2)}\left(a\delta_{hl} - \sqrt{\frac{2}{3}}p_l(a)\delta_{h1}\right); l \neq 1, \tag{39}$$

where δ_{hl} is the Kronecker delta

$$\delta_{ij} = \begin{cases} 1; & i = j \\ 0; & i \neq j. \end{cases}$$

When $h = l = 1$, the coefficient $\mathbf{G}_{11}$ can be calculated directly and equals

$$\mathbf{G}_{11} = -\frac{7}{9} + \frac{2}{3}\log 2 - \frac{1}{3}\log(1-a^2). \tag{40}$$

The simple form of $\mathbf{G}_{hl}$ leads to a very sparse matrix $\mathbf{A}$ with non-zero entries only along its first row and first column and its main diagonal. Although the size of the matrix $\mathbf{A}$ needs to be large for accurate calculation of the eigenvalues and eigenvectors, fortunately only those few eigenvalues and eigenvectors that describe the lower modes of oscillation are needed. Hence, an Arnoldi iteration based method[32] is used to efficiently compute the few lowest eigenvalues and the corresponding eigenvectors.

When $a = \pm 1$ or $a = 0$, Green's functions (36) diverge. A mathematical analysis of these limiting cases are outside the scope of this study. However, it was observed computationally that the algorithm for determining the eigenvalues of matrix $\mathbf{A}$ was convergent as $a \to 0$.

V. RESULTS

In this section, results are reported from calculations of eigenmodes and eigenfrequencies using both methods for situations mimicking a constrained liquid drop in ambient air, viz. ($\rho_e \ll \rho_i \equiv \rho$). Free surface profiles of a drop constrained at $a = 0$ that is undergoing mode 2 oscillations and where the eigenmode shapes have been obtained using the minimization method and Green's function method are shown in Figures 3 and 4, respectively, at various orders of approximation using different numbers N of basis functions. In both figures, the differences in free surface shapes obtained using different values of N far from the contact point are indistinguishable as the order of the approximation is increased. However, in the neighborhood of the contact point, not only does the computed shape vary with the order of the approximation used but also with the analytical method that is employed to calculate it. As can be readily seen from in Figure 3, the free surface profile calculated using the minimization technique becomes sharper or takes on a pointed appearance in the vicinity of the contact point as the order of the approximation or the number N of basis functions used is increased. When N is sufficiently large, the tangent to the free surface profile appears discontinuous as the pinning point is approached from either side of it. Such a discontinuity in the tangent to the drop profile has also been observed in experiments on oscillations of capillary switches held by a plate or a tube of finite thickness (cf. Figure 1) by Theisen *et al.*[27]

Similar behavior in the vicinity of the contact point is also observed in mode shapes calculated using the Green's function method at high orders of approximation. The mode shapes at lower orders, however, differ from those calculated with the minimization method. In fact, the pinned contact condition is not well satisfied for mode shapes calculated with Green's function method when too few basis functions are used. This defect arises because of the way the pinned contact line condition is imposed in Green's function method. In this method, the fixed contact condition is specified

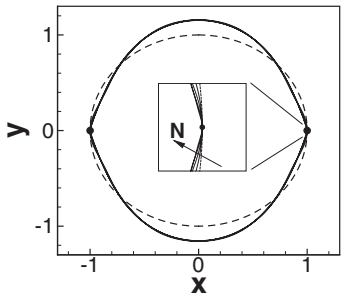

FIG. 3. The drop shape corresponding to the second mode of oscillation. Here, the eigenmode and the corresponding eigenvalue (not shown) have been calculated using the minimization method. In this figure and in Figure 4, drop shapes are shown for calculations made with $N = 10$, 25, 50, and 100 Legendre polynomials. In Figures 3, 4, and 7, the solid curves —— represent the drop shapes and the dashed curves - - - represent the unperturbed equilibrium shapes of the drops. In both Figures 3 and 4, since drop shapes calculated with different numbers of basis functions cannot be distinguished from one another when the whole drop is viewed, the insets show blowups of the free surface shapes in the vicinity of the pinning points.

through Green's function (Eq. (36)) which is then expanded in a series of Legendre polynomials. Therefore, with this method, the fixed contact point condition is satisfied asymptotically as the order of the approximation increases.

For the situation considered in Figures 3 and 4 where a drop pinned at $a = 0$ is undergoing second mode oscillations, the variation of the square of the dimensionless frequency of oscillation with the order of approximation N is shown in Figure 5. This figure makes plain that the frequencies calculated by the minimization method asymptotically approach a constant value, the value of the mode 2 frequency, as N increases. The Green's function method too predicts the same asymptotic value of the modal frequency but does so while using a very low order of approximation in spite of violation of the pinning condition at low N (see above). Indeed, the right value of the modal frequency is predicted with the Green's function method with a value of N as low as 5. Figure 5 shows that the asymptotic value of the mode 2 frequency is lower than that reported by Bostwick and Steen.[23] Due to computational limitations of their approach, Bostwick and Steen[23] used only 13 polynomials in constructing their modal shapes. Reassuringly, Figure 5 also shows that the minimization method of this paper predicts the same value of the modal frequency reported by Bostwick and Steen[23] when only 13 polynomials are used in the approximation. Therefore, it would be safe to presume that Bostwick and Steen's[23] approach would also predict the exact frequencies if it would not have been prohibitively expensive for them to deploy higher orders of approximation than those that they used to obtain their results.

Figure 6 shows the variation of the square of the dimensionless frequencies of modes 1, 2, and 3 with the order of approximation for a drop pinned at $a = 0.577$. As made evident by Figure 6, the variation of the frequency with N for modes 1 and 3 when $a = 0.577$ is quite similar to the

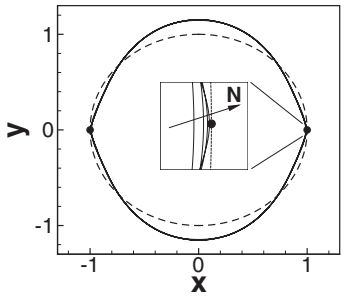

FIG. 4. The drop shape corresponding to the second mode of oscillation. Here, the eigenmode and the corresponding eigenvalue (not shown) have been calculated using the Green's function method.

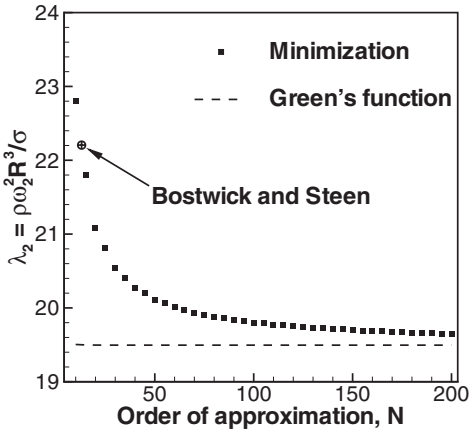

FIG. 5. Variation of the square of the dimensionless frequency λ_2 of the second mode of oscillation of a droplet pinned at $a = 0$ with the order of approximation N. In Figures 5 and 6, points correspond to results obtained with the minimization method (labeled "Minimization") and the dashed curve corresponds to results obtained with the Green's function method (labeled "Green's function"). Also shown here is the value of the eigenvalue obtained by Bostwick and Steen[23] using 13 polynomials (labeled "Bostwick and Steen").

case discussed previously when $a = 0$. However, when $a = 0.577$, both analytical methods predict the same frequency of $\sqrt{\lambda} = \sqrt{8}$ for a constrained drop undergoing mode 2 oscillations, which also happens to equal the frequency of a free drop undergoing mode 2 oscillations. As explained by Bostwick and Steen,[23] $a = 0.577$ is a solution of $P_2(a) = 0$ or a node of the second Legendre polynomial P_2. Since the amplitude of the perturbation is always zero at a node, constraining a free drop at a node does not affect its oscillatory response. Hence, the frequencies of oscillation of free and constrained drops are identical whenever the constraint is located at a node of the corresponding Rayleigh mode. Moreover, because the second eigenmode of a free drop is given by the second Legendre polynomial, higher order approximations are not required to describe this mode.

For the situations considered in the previous paragraph, eigenvector calculations using either method also confirm that the coefficient corresponding to P_2 is the only non-zero term in the expansion of the surface perturbation of a constrained drop undergoing mode 2 oscillations. Free surface shapes for the first three modes of oscillations for a drop pinned at $a = 0.577$ are provided in Figure 7. From examination of the mode shapes and corresponding modal frequencies in this and other cases, it has been found that $N = 100$ is sufficiently large to accurately describe the dynamics of the lower modes of oscillation. Indeed, further increases in the value of N change the

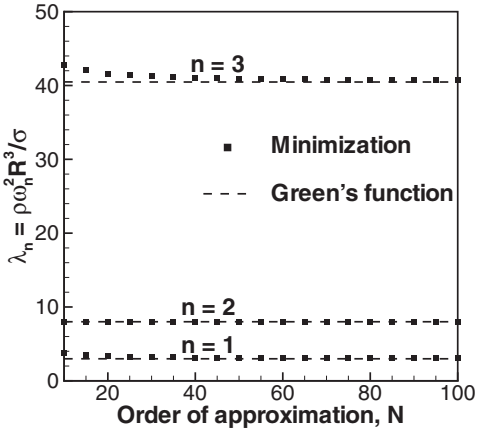

FIG. 6. Variation of the square of the dimensionless frequency λ_n of the first, second, and third modes of oscillation of a droplet pinned at $a = 0.577$ with the order of approximation N.

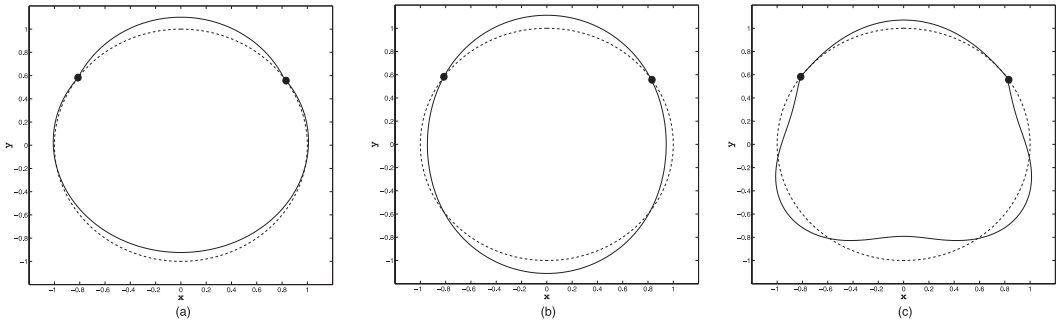

FIG. 7. Drop shapes corresponding to the (a) first, (b) second, and (c) third modes of oscillation for a droplet pinned at $a = 0.577$.

computed values of the modal frequencies by less than 2%. Therefore, henceforward, all results to be reported have been generated by approximating the surface perturbation z with $N = 100$ Legendre polynomials.

The square of the frequency for the first three modes of oscillation are plotted as a function of the position of the contact circle, a, along with the corresponding Rayleigh frequencies and those reported by Bostwick and Steen in Figure 8. As predicted by the implicit expression of Eq. (31), the eigenvalues of the constrained problem always lie between the corresponding and successive Rayleigh frequencies. Eigenvalues calculated by the minimization method and Green's function method are identical, whereas for reasons explained earlier, Bostwick and Steen's method predicts values greater than or equal to ours. When the contact circle is located at the fixed point of a free drop oscillation, all three methods predict the same frequency which is the corresponding Rayleigh frequency. The maximum difference between our approaches and Bostwick's occurs when the deviation from the Rayleigh frequency is the most.

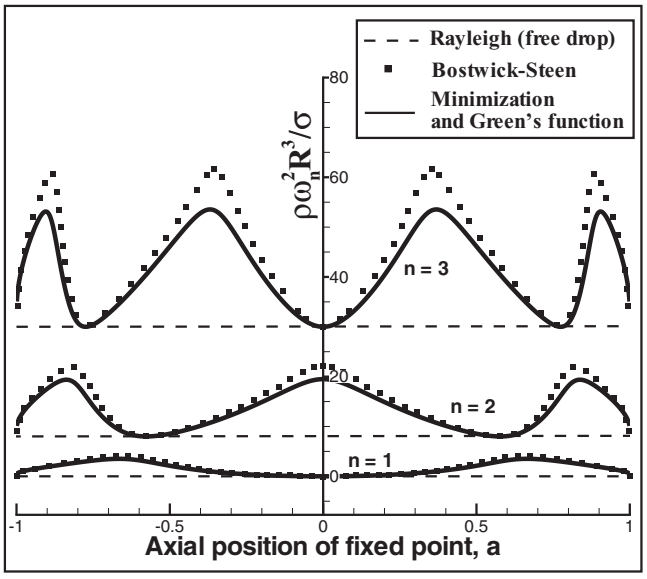

FIG. 8. Variation of the eigenvalues, or the squares of the dimensionless frequencies, of the first, second, and third modes of oscillation of droplets as a function of the pinning position a. The horizontal dashed lines - - - correspond to eigenvalues of the Rayleigh modes (labeled as "Rayleigh (free drop)"). The points denote results obtained by Bostwick and Steen[23] (labeled "Bostwick-Steen"). The solid curves —— represent results obtained in this paper using the two methods (labeled "Minimization and Green's function").

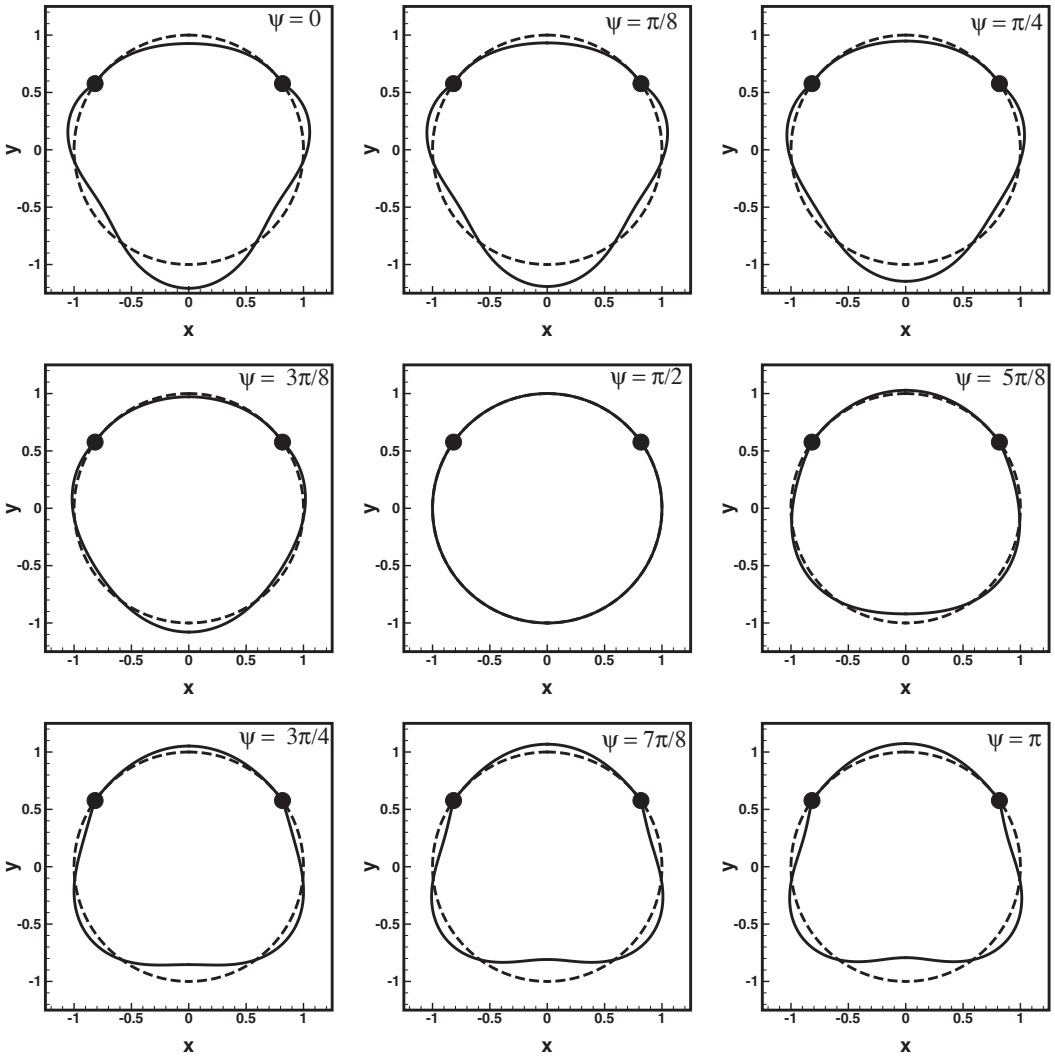

FIG. 9. Transient shapes (shown as solid curves) of an oscillating drop pinned at $a = 0.55$ and undergoing mode 3 oscillations. In each panel, the shape of the unperturbed drop is shown as a dotted curve. Starting from the earliest time at the top left and proceeding left to right in each row, the transient shapes in each panel correspond to drop shapes that result at successive phase angles ψ that differ by $\omega\Delta t = \pi/8$ with the unperturbed shape arbitrarily assigned a phase angle of $\psi = \pi/2$. The sequence shown corresponds to one half of a period of oscillation. In the second half of the period, shapes at increasing values of the phase angle, or time, are those that would result by starting at the bottom right and proceeding right to left in each row.

The transient shape for each mode can be calculated by substituting the corresponding mode shape function, $z(x)$ or $z(\theta)$, in Eq. (14) and then the shape perturbation η in Eq. (4). A sequence of transient shapes for one such case, viz., a drop pinned at $a = 0.55$ and undergoing mode 3 oscillations, is shown in Figure 9. Although the current analysis is applicable only to linear perturbations such that $\eta/R \ll 1$, Figure 9 uses a larger perturbation to better contrast the perturbed (solid) and unperturbed (dashed) drop shapes. Since the oscillations are harmonic in nature, the drop shapes repeat themselves after every time interval, Δt, such that $\omega\Delta t = 2\pi$. The phase angle, ψ, is defined as $\psi = \omega\Delta t$; $0 \le \psi \le 2\pi$. In Figure 9, the transient shape for which the surface perturbation is a maximum at $\theta = \pi$, i.e., the bottom, is arbitrarily chosen as $\psi = 0$. The velocity field vanishes everywhere within the drop at this instant in time. During the next half of a period of oscillation that is depicted in Figure 9, $0 \le \psi \le \pi$, the velocity field above the contact point is in the upward direction. At $\psi = \pi/2$, the surface perturbation vanishes instantaneously and the drop is identically spherical in shape. Subsequently, the drop surface above the contact point continues to increase in height until it reaches a maximum

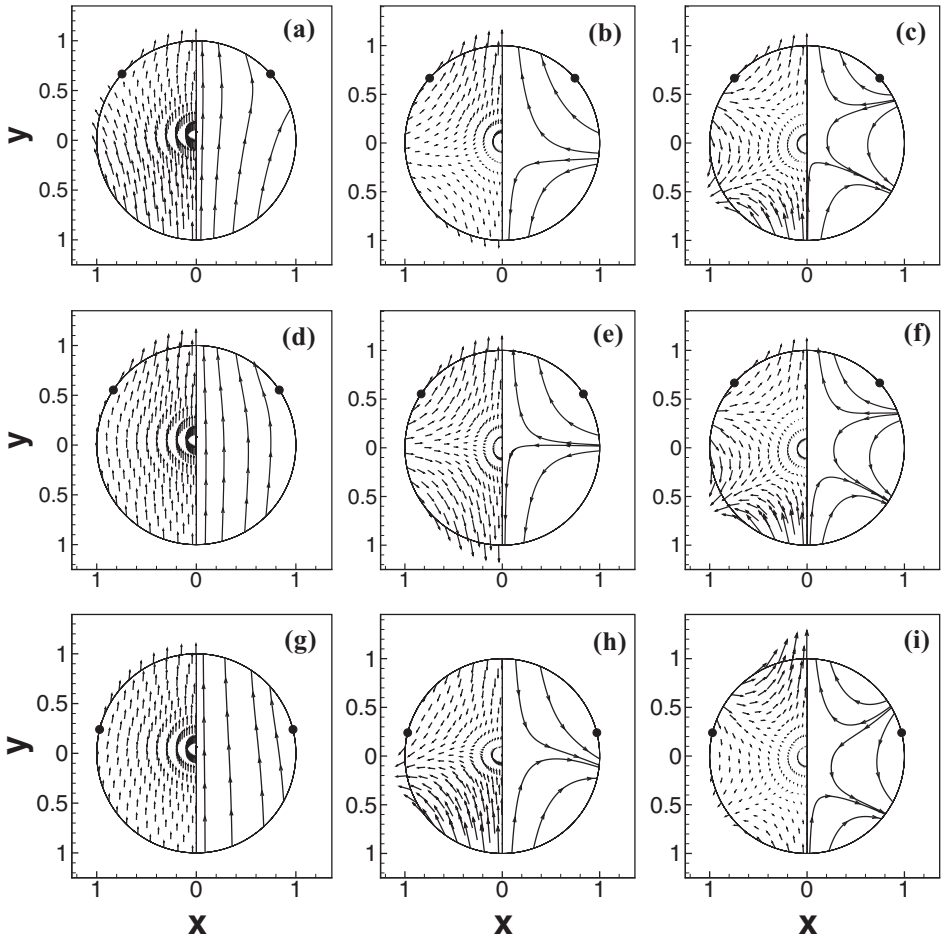

FIG. 10. Velocity vectors (shown on the left of the axis of symmetry) and streamlines (shown on its right) inside oscillating drops pinned at an azimuth at the instant when the surface perturbation vanishes. The rows correspond to fixed values of the pinning location such that $a = 0.67$ in (a)–(c), $a = 0.55$ in (d)–(f), and $a = 0.24$ in (g)–(i). Each column corresponds to a given mode such that the drop is undergoing mode 1 oscillations in (a), (d), and (g), mode 2 oscillations in (b), (e), and (h), and mode 3 oscillations in (c), (f), and (i). Because of axial symmetry, each figure depicts the drop shape and the flow field in a cross sectional plane including the axis of symmetry.

at $\psi = \pi$. The velocity field vanishes everywhere within the drop once again at this instant in time. In the second half of the period of oscillation that is not shown in Figure 9, $\pi \leq \psi \leq 2\pi$, the drop would trace the same sequence of shapes that is shown in Figure 9 albeit by proceeding from the bottom right to the top left. During this time period, the drop would once again pass through a state of zero surface perturbation when $\psi = 3\pi/4$ but the velocity field above the point of contact would be in the downward direction for $\pi < \psi < 2\pi$.

The velocity field inside an oscillating drop can be calculated from the gradient of the velocity potential, $\mathbf{v} = -\nabla\phi^i$, where ϕ^i is obtained from Eq. (15) after plugging into it the corresponding surface perturbation function $z_k(x)$ for mode k. Velocity vectors and streamlines are shown in Figure 10 inside drops constrained at $a = 0.67$, 0.55, and 0.24 that are vibrating in the first three modes, $k = 1$, 2, and 3, of oscillations. In this figure, each row corresponds to a fixed value of a and each column corresponds to a fixed mode number. For drops undergoing mode 1 oscillations, Figure 10 shows that the dynamics are predominantly axial. Close inspection of Figure 10 further shows that near the solid contact within such drops, the streamlines bend in the direction tangent to the free surface due to the vanishing of the normal component of the velocity at the pinning point (cf. Eq. (10)). Although the streamlines within the drops undergoing modes 2 and 3 oscillations are similar to those within free drops undergoing Rayleigh oscillations, Figure 10 shows that the

velocity fields are asymmetric about the location of the solid contact. For example, in Figure 10(i), the flow is stronger, i.e., the magnitude of the velocity vectors is large, in the part of the drop which lies above the solid contact compared to that which lies below it where the fluid is nearly quiescent. Thus, by pinning a drop, it should be possible to selectively excite just a portion of a drop's surface.

VI. CONCLUSIONS

In this paper, the integro-differential eigenvalue problem (23) governing the linear oscillations of a spherical drop that is constrained at an azimuth is analyzed. The problem solved is similar to that governing the classic Rayleigh oscillations of a free drop except in the present problem the formulation is augmented relative to the Rayleigh problem by an additional constraint that enforces the vanishing of the surface perturbation along the circle of contact where the drop is pinned to the ring of vanishingly small thickness. Here, two analytical solution methodologies are used to determine the eigenvalues and eigenfunctions of this linear operator problem. The first approach, termed the minimization method, uses a modified Rayleigh-Ritz method, and finds functions that minimize a certain scalar functional and satisfy all constraints. By choosing Legendre polynomials of order greater than zero as basis functions, the volume constraint and boundedness conditions are satisfied. The vanishing of the surface perturbation at the solid contact is ensured by including it in the formulation by means of a Lagrange multiplier. The self-adjointness of the linear operators is exploited to come up with a solution methodology that is both elegant and computationally inexpensive. An implicit expression for the eigenvalues (the square of the non-dimensional mode frequencies) is derived which conclusively proves that the mode frequencies of the constrained drop lie between the corresponding and successive mode frequencies of a free drop.

The second approach, termed Green's function method, involves the derivation of an appropriate composite Green's function that satisfies all the boundary conditions. Following the methodology outlined by Strani and Sabetta,[22] various eigenmodes are identified. The Green's function method, as the minimization method, uses Legendre polynomials as a basis function set to represent the deformation of the free surface. Computational results obtained with both methods have shown that a linear combination of the first 100 Legendre polynomials is sufficient to predict accurately the mode shapes and their frequencies.

Bostwick and Steen[23] have studied the same problem as in this work but comparison of the present results with those of Bostwick and Steen[23] point to some differences between their and the new results with respect to modal frequencies and mode shapes in the vicinity of the contact point. Due to computational difficulties, Bostwick and Steen[23] used a basis set consisting of 13 Legendre polynomials, a number that is shown in this work to be too small in general to enable prediction of oscillation modes with quantitative accuracy. Interestingly, mode shapes predicted by both analytical methods used here also show a near discontinuity in the tangent to the free surface just above and below the solid contact despite the smooth nature of the basis functions, a phenomenon that is akin to that which is observed when a Fourier decomposition of a square wave is carried out. Indeed, Bostwick and Steen[23] have pointed out that such discontinuities were observed by Theisen *et al.*[27] in their experimental investigation of the center-of-mass motion of two spherical caps that are separated by a plate of finite thickness.

ACKNOWLEDGMENTS

This research was sponsored by the Basic Energy Sciences (BES) program of the (U.S.) Department of Energy (DOE) (Grant No. DE-FG02-96ER14641). Acknowledgment is also made to the Donors of the American Chemical Society Petroleum Research Fund for partial support of this research. Santhosh Ramalingam held a Bilsland Dissertation Fellowship at Purdue while carrying out a portion of this research. The senior author (O.A.B.) learned about capillary switches during a seminar visit by Professor Paul Steen of Cornell to Purdue. The authors are profoundly grateful to Professor Amir Hirsa of Rensselaer Polytechnic Institute (RPI) for exposing them to potential applications of double droplet systems and getting them interested in the oscillations of such systems.

APPENDIX: GREEN'S FUNCTION EIGENVALUE PROBLEM

Using the definitions described in Eq. (24) we may evaluate part of the integral appearing in Eq. (32) to be

$$\begin{aligned}\mathbf{M}z(x) &= \phi_0 + \sum_{k=1}^{\infty} \beta_k p_k(x) \int_{-1}^{1} z(\xi) p_k(\xi) d\xi \\ &= \phi_0 + \int_{-1}^{1} \Gamma(x,\xi) z(\xi) d\xi, \end{aligned} \tag{A1}$$

where

$$\Gamma(x,\xi) = \sum_{k=1}^{\infty} \beta_k p_k(x) p_k(\xi). \tag{A2}$$

Substituting Eq. (A1) in Eq. (32) yields

$$z(x) = \lambda \left[\phi_0 \int_{-1}^{1} G(x,y) dy + \int_{-1}^{1} \int_{-1}^{1} G(x,y) \Gamma(y,\xi) z(\xi) dy d\xi \right]. \tag{A3}$$

The constant ϕ_0 can now be evaluated by imposing the volume constraint, i.e., substituting the above equation in (22a). Thus

$$\phi_0 = \frac{-\int_{-1}^{1}\int_{-1}^{1}\int_{-1}^{1} G(x,y)\Gamma(y,\xi) z(\xi) dx dy d\xi}{\int_{-1}^{1}\int_{-1}^{1} G(x,y) dx dy},$$

Eq. (A3) can now be rewritten as

$$z(x) = \lambda \int_{-1}^{1} K(x,\xi) z(\xi) d\xi, \tag{A4}$$

where

$$K(x,\xi) = -\frac{\int_{-1}^{1}\int_{-1}^{1}\int_{-1}^{1} G(x,y) G(v,\tau) \Gamma(\tau,y) dy dv d\tau}{\int_{-1}^{1}\int_{-1}^{1} G(\tau,y) d\tau dy} + \int_{-1}^{1}\int_{-1}^{1} G(x,y)\Gamma(y,\xi) dy. \tag{A5}$$

By expanding $z(x)$ and $K(x,\xi)$ in terms of normalized Legendre polynomials as shown below, Eq. (A4) can be reduced to an infinite system of linear algebraic equations

$$z(x) = \sum_{k=1}^{\infty} z_k p_k(x); \qquad z_k = \langle z, p_k \rangle \tag{A6}$$

and

$$K(x,\xi) = \sum_{h,l=1}^{\infty} \mathbf{K}_{hl}\ p_h(x) p_l(\xi).$$

Note that p_0 term has been dropped as result of volume constraint. The terms $\mathbf{K}_{hl}$ can be obtained from the corresponding terms in $G(x,\xi)$,

$$G(x,\xi) = \sum_{h,l=0}^{\infty} \mathbf{G}_{hl} p_h(x) p_l(\xi), \tag{A7a}$$

$$\mathbf{G}_{hl} = \mathbf{G}_{lh} = \langle \langle G, p_h \rangle, p_l \rangle. \tag{A7b}$$

Substituting the above expansion along with Eq. (A2) in the definition for $K(x,\xi)$ (A5) we get

$$\mathbf{K}_{hl} = \beta_l \left(\mathbf{G}_{hl} - \frac{\mathbf{G}_{0l}\mathbf{G}_{h0}}{\mathbf{G}_{00}} \right). \tag{A8}$$

Using this expression for $\mathbf{K}_{hl}$ in (A4) the terms of $z(x)$ can be found to satisfy the following linear algebraic equations:

$$z_h = \lambda \sum_{l=1}^{\infty} \beta_l \left(\mathbf{G}_{hl} - \frac{\mathbf{G}_{0l}\mathbf{G}_{h0}}{\mathbf{G}_{00}} \right) z_l.$$

Using the following change in variables:

$$\zeta_h = \sqrt{\beta_h} z_h, \text{ and } \alpha = \frac{1}{\lambda}$$

the system of algebraic equations can be rewritten as

$$\alpha \zeta_h = \sum_{l=1}^{\infty} \mathbf{A}_{hl} \zeta_l, \tag{A9}$$

where

$$\mathbf{A}_{hl} = \mathbf{A}_{lh} = \sqrt{\beta_h \beta_l} \left(\mathbf{G}_{hl} - \frac{\mathbf{G}_{0l}\mathbf{G}_{h0}}{\mathbf{G}_{00}} \right).$$

As $\mathbf{A}$ is a self-adjoint matrix, the eigenvalues α and hence λ are real.

[1] L. E. Scriven, "Drops and bubbles: Their science and the systems they model," in *Proceedings of the International Colloquium on Drops and Bubbles*, edited by D. J. Collins, M. S. Plesset, and M. M. Saffren (California Institute of Technology, 1974), pp. xii–xxviii.
[2] L. Rayleigh, "On the capillary phenomena of jets," Proc. R. Soc. London **29**, 71–97 (1879).
[3] H. Lamb, *Hydrodynamics* (Dover, 1932).
[4] S. Chandrasekhar, *Hydrodynamic and Hydromagnetic Stability* (Clarendon, Oxford, 1961).
[5] F. H. Busse, "Oscillation of a rotating liquid-drop," J. Fluid Mech. **142**, 1–8 (1984).
[6] T. W. Patzek, O. A. Basaran, R. E. Benner, and L. E. Scriven, "Nonlinear oscillations of two-dimensional, rotating inviscid drops," J. Comput. Phys. **116**, 3–25 (1995).
[7] C. A. Miller and L. E. Scriven, "Oscillations of a fluid droplet immersed in another fluid," J. Fluid Mech. **32**, 417 (1968).
[8] A. Prosperetti, "Normal-mode analysis for the oscillations of a viscous-liquid drop in an immiscible liquid," J. de Mécanique **19**, 149–182 (1980).
[9] O. A. Basaran, T. C. Scott, and C. H. Byers, "Drop oscillations in liquid-liquid systems," AIChE J. **35**, 1263–1270 (2004).
[10] J. A. Tsamopoulos and R. A. Brown, "Non-linear oscillations of inviscid drops and bubbles," J. Fluid Mech. **127**, 519–537 (1983).
[11] T. S. Lundgren and N. N. Mansour, "Oscillation of drops in zero gravity with weak viscous effects," J. Fluid Mech. **194**, 479–510 (1988).
[12] T. W. Patzek, R. E. Benner, O. A. Basaran, and L. E. Scriven, "Nonlinear oscillations of inviscid free drops," J. Comput. Phys. **97**, 489–515 (1991).
[13] O. A. Basaran, "Nonlinear oscillations of viscous-liquid drops," J. Fluid Mech. **241**, 169–198 (1992).
[14] R. Apfel, Y. Tian, J. Jankovsky, T. Shi, X. Chen, R. Holt, E. Trinh, A. Croonquist, K. Thornton, A. Sacco, C. Coleman, F. Leslie, and D. Matthiesen, "Free oscillations and surfactant studies of superdeformed drops in microgravity," Phys. Rev. Lett. **78**, 1912–1915 (1997).
[15] E. I. Franses, O. A. Basaran, and C. H. Chang, "Techniques to measure dynamic surface tension," Curr. Opin. Colloid Interface Sci. **1**, 296–303 (1996).
[16] O. A. Basaran and D. W. Depaoli, "Nonlinear oscillations of pendant drops," Phys. Fluids **6**, 2923–2943 (1994).
[17] E. D. Wilkes and O. A. Basaran, "Drop ejection from an oscillating rod," J. Colloid Interface Sci. **242**, 180–201 (2001).
[18] M. Francois and W. Shyy, "Micro-scale drop dynamics for heat transfer enhancement," Prog. Aerosp. Sci. **38**, 275–304 (2002).
[19] D. Mampallil, D. van den Ende, and F. Mugele, "Controlling flow patterns in oscillating sessile drops by breaking azimuthal symmetry," App. Phys. Lett. **99**, 154102 (2011).
[20] M. J. Vogel, P. Ehrhard, and P. H. Steen, "The electroosmotic droplet switch: Countering capillarity with electrokinetics," Proc. Natl. Acad. Sci. U.S.A. **102**, 11974–11979 (2005).
[21] A. H. Hirsa, C. A. Lopez, M. A. Laytin, M. J. Vogel, and P. H. Steen, "Low-dissipation capillary switches at small scales," Appl. Phys. Lett. **86**, 014106 (2005).
[22] M. Strani and F. Sabetta, "Free-vibrations of a drop in partial contact with a solid support," J. Fluid Mech. **141**, 233–247 (1984).
[23] J. B. Bostwick and P. H. Steen, "Capillary oscillations of a constrained liquid drop," Phys. Fluids **21**, 032108 (2009).
[24] E. D. Wilkes and O. A. Basaran, "Forced oscillations of pendant (sessile) drops," Phys. Fluids **9**, 1512–1528 (1997).
[25] E. D. Wilkes and O. A. Basaran, "Hysteretic response of supported drops during forced oscillations," J. Fluid Mech. **393**, 333–356 (1999).
[26] D. V. Lyubimov, T. P. Lyubimova, and S. V. Shklyaev, "Behavior of a drop on an oscillating solid plate," Phys. Fluids **18**, 012101 (2006).

[27] E. A. Theisen, M. J. Vogel, C. A. Lopez, A. H. Hirsa, and P. H. Steen, "Capillary dynamics of coupled spherical-cap droplets," J. Fluid Mech. **580**, 495–505 (2007).
[28] D. M. Slater, C. A. Lopez, A. H. Hirsa, and P. H. Steen, "Chaotic motions of a forced droplet-droplet oscillator," Phys. Fluids **20**, 092107 (2008).
[29] S. Ramalingam and O. A. Basaran, "Axisymmetric oscillation modes of a double droplet system," Phys. Fluids **22**, 112111 (2010).
[30] D. Ramkrishna and N. R. Amundson, *Linear Operator Methods in Chemical Engineering* (Prentice-Hall, Upper Saddle River, NJ, 1985).
[31] T. M. MacRobert, *Spherical Harmonics* (Methuen, London, 1947).
[32] W. E. Arnoldi, "The principle of minimized iterations in the solution of the matrix eigenvalue problem," Q. Appl. Math. **9**, 17–29 (1951).